The 3D DC sensitivity for surface and subsurface sources

Klaus Spitzer[1]

École Polytechnique
P.O.Box 6079, Succ. Centre-Ville, Montreal (QC) H3C 3A7, Canada

1 Introduction

The DC sensitivity is a substantial and meaningful quantity in any data interpretation process. It indicates the change in potential due to the change in resistivity of a cell volume. For inversion schemes, it provides a link between data and model vector in terms of the Jacobian matrix. It is also very useful for the interpretation of field data using forward modeling, enabling the modeler to assess the resolvability of certain model parameters (Spitzer and Kümpel, 1997). Practitioners might find it helpful for planning field surveys and choosing optimal source configurations with respect to their targets. While the spatial sensitivity distribution for surface source configurations is found sporadically in the literature, the one for subsurface sources is lacking. Sensitivity studies were carried out by several authors usually in conjunction with inversion techniques. McGillivray and Oldenburg (1990) depict the sensitivity as an example for a single pole source at the surface for a 1D and 2D case and show the distortion of the sensitivity for a 2D prismatic body. Boerner and West (1989) deduce Fréchet derivatives in the sense of single scattering theory and compare their evolved DC expression with the one for a 1D earth described by Oldenburg (1978). Sasaki (1994) shows a coarse 3D sensitivity plot for a surface dipole-dipole configuration using two orthogonal sections through 3D space. Also Noel and Xu (1991) present a vertical section for a dipole-dipole arrangement at the surface. A sensitivity study using small 3D grids was carried out by Park and Van (1991). An early work on sensitivities for the homogeneous earth (then called signal contribution sections) was performed by Barker (1979). He investigated the sensitivities for surface four-electrode arrangements and particularly pointed out the differences for Wenner, Schlumberger and several Dipole-Dipole combinations. Weller et al. (1996) derive an expression for the pole-pole sensitivity in a closed volume bounded by an isolator and show that sensitivities may be superposed for multi-electrode arrangements.

Four different schemes are briefly outlined for calculating the sensitivity in 3D. For arbitrary conductivity structures, the sensitivity may be calculated by numerical DC forward modeling using a source at the transmitter and a fictitious source at the receiver location. A separate numerical approach has been developed solving the partial differential equation defining the sensitivity problem. Another method using two DC forward runs employs the perturbation of a resistivity block to derive the sensitivity and last but not least an analytical solution is available for the homogeneous halfspace, .

Following that, an example is shown of the 3D sensitivity distribution for a subsurface pole-pole arrangement in a homogeneous earth. The results are displayed using two orthogonal sections. Distinct regions of negative sensitivities do always occur; blocks within these regions affect the overall response in an apparently paradoxical but physically reasonable manner: a well conducting block in a region of negative sensitivities increases the apparent resistivity response whereas a highly resistive block has the opposite effect. Most notably, for buried, horizontal electrode arrangements, the negatively sensitive regions form tube-shaped, cylindrical structures opening towards the surface whereas a vertical arrangement

[1]now at: Geowissenschaftliche Gemeinschaftsaufgaben, Stilleweg 2, 30655 Hannover, e-mail: klaus.spitzer@bgr.de

yields a closed, spherical one. Finally, it is investigated, how varying conductivity contrasts influence the sensitivity. A more comprehensive illustration is given in the full paper that is going to be published in Geophysical Journal International.

2 The Sensitivity

The DC sensitivity Φ is the derivative of the measured potential with respect to the resistivity assigned to a volume or block within the model space. For a fixed source position, it reads as

$$\Phi_{lmn} = \frac{\partial V_m}{\partial \rho_n} \quad , \tag{1}$$

where V_m is the potential at grid node m, ρ_n is the resistivity assigned to the n^{th} block, $n = 1, \ldots, \tilde{N}$, and $\tilde{N}$ is the number of model blocks. l is the index for the source location so that Φ_{lmn} reads as the sensitivity at node m with respect to a change in resistivity in cell n and a source located at node l. For one source location l, the sensitivity matrix containing the sensitivities at all nodes m with respect to all resistivity blocks n is an $N \times \tilde{N}$ matrix of the form

$$\Phi_l = \begin{pmatrix} \frac{\partial V_1}{\partial \rho_1} & \cdots & \frac{\partial V_1}{\partial \rho_{\tilde{N}}} \\ \vdots & & \vdots \\ \frac{\partial V_N}{\partial \rho_1} & \cdots & \frac{\partial V_N}{\partial \rho_{\tilde{N}}} \end{pmatrix} \quad . \tag{2}$$

A row of the matrix contains the derivatives at one receiver position with respect to all resistivity blocks, whereas a column consists of the derivatives at all grid nodes with respect to one resistivity block. In other words, a row contains information on the sensitivity throughout the halfspace for a particular electrode configuration. This is of special concern, if, e.g., the high resolution region for a given transmitter/receiver arrangement is sought. On the other hand, the columns contain the sensitivities for all receivers with respect to a fixed volume. They are to be considered, if a-priori information on the location of a target body exists and the optimum resolution electrode configuration is to be designed.

Three of the four methods described in the following are numerical ones being apt to determine the sensitivity for arbitrary conductivity structures, while one is analytical and only for homogeneous cases. Generally, the whole sensitivity matrix may be calculated by each of the methods. The FD methods, however, provide with each run only one row or one column, respectively, so that the whole matrix is obtained by repetitive application. For many problems, though, the supply of a single column or row is sufficient. The choice of the appropriate method is therefore important to yield computational efficiency.

2.1 Calculation of the Sensitivity by DC Forward Modeling

Expressing the conservative electrical field $\boldsymbol{E}$ as the negative gradient of the scalar potential V

$$\boldsymbol{E} = -\nabla V \tag{3}$$

and using Ohm's law

$$\boldsymbol{j} = \sigma \boldsymbol{E} \tag{4}$$

we can write the current density $\boldsymbol{j}$ as

$$\boldsymbol{j} = -\sigma \nabla V \quad . \tag{5}$$

The gradient ∇V can now be approximated by a central FD expression. As an example, the FD term for the x-direction in irregular grids reads as

$$\left.\frac{\partial V}{\partial x}\right|_{i,j,k} = \frac{f_{i-1}^2 V_{i+1,j,k} + (f_i^2 - f_{i-1}^2) V_{i,j,k} - f_i^2 V_{i-1,j,k}}{f_{i-1} f_i (f_{i-1} + f_i)} \tag{6}$$

where f_i and f_{i-1} are the grid spacings adjacent to node (i,j,k). A similar expression is obtained for y and z. The conductivity σ of an infinitesimal cell volume at the grid node (i,j,k) is approximated by a volume-weighted arithmetic mean over neighboring grid cells according to Brewitt-Taylor and Weaver (1976). For details see the finite difference approach by Spitzer (1995).

The sensitivity for a defined transmitter and receiver configuration can be expressed as the inner product of the current densities $\boldsymbol{j}^l$ and $\boldsymbol{j}^m$ produced by a current source of strength I at the transmitter l and receiver position m, respectively, integrated over the perturbed volume τ_n. The applied current I is usually of unit strength. This definition goes back to a formulation by Geselowitz (1971) and is well described, e.g., by Park & Van (1991). It reads as

$$\Phi_{lmn} = \frac{1}{I} \iiint_{\tau_n} \boldsymbol{j}^l \, \boldsymbol{j}^m \, d\tau_n \quad , \tag{7}$$

where the current densities $\boldsymbol{j}^l$ and $\boldsymbol{j}^m$ are calculated using the finite difference expression according to eqs (5) and (6). Mathematically, the sensitivity theorem can be derived from the bilinear identity described by Lanczos (1961), which is closely related to the Green's functions and Green's identities.

For a given transmitter and receiver position, two separate forward runs have to be carried out locating a source subsequently at the transmitter and the receiver position. Thus, the sensitivity is provided throughout the whole volume with respect to one transmitter/receiver configuration. With other words, the index m in eq. (1) remains fixed, whereas n runs through all values giving one *row* of the sensitivity or Jacobian matrix in eq. (2).

2.2 Sensitivity Forward Modeling

Another way of determining sensitivities is a separate finite difference approach solving a set of partial differential equations defining the sensitivity problem.

The procedure is based on a technique proposed by Smith & Vozoff (1984) who derive the symmetric and positive definite set of linear equations

$$\mathbf{A}\boldsymbol{v} = \boldsymbol{b} \tag{8}$$

with respect to one block conductivity σ_n. $\mathbf{A}$ is the coefficient matrix arising from a finite difference approach of the geoelectric problem, $\boldsymbol{v}$ is the unknown vector of the potentials V_m and $\boldsymbol{b}$ denotes the source term. The derivative reads as

$$\mathbf{A}\frac{\partial \boldsymbol{v}}{\partial \sigma_n} = -\frac{\partial \mathbf{A}}{\partial \sigma_n}\boldsymbol{v} \quad , \tag{9}$$

since $\partial \boldsymbol{b}/\partial \sigma_n = 0$. $\partial \mathbf{A}/\partial \sigma_n$ is determined easily by setting all cell conductivities equal to 1 within the relevant model block. All other conductivities are set to 0. The system of linear equations of eq. (8) is solved for the potential $\boldsymbol{v}$ using an efficient SSOR-preconditioned conjugate gradient method (SSOR: Successive overrelaxation method; Spitzer, 1995; Hestenes & Stiefel, 1952). Then the right side of eq. (9) consists of only one matrix–vector multiplication. The obtained set of equations is of the form of eq. (8) which is again solved by the conjugate gradient method yielding the vector $\partial \boldsymbol{v}/\partial \sigma_n$. The sensitivity as

defined in eq. (1) is obtained in a straightforward way by multiplying $\partial v/\partial\sigma_n$ by the factor $-\sigma_n^2$ giving the required sensitivity for node m

$$\frac{\partial V_m}{\partial \rho_n} = -\frac{\partial V_m}{\partial \sigma_n}\sigma_n^2 \quad . \tag{10}$$

Thus, for the sensitivity matrix's first column, two forward calculations are necessary. For each additional conductivity block, the numerical amount of work is reduced to only one forward run once the potential v is determined. In contrast to the method described in section 2.1, we obtain the sensitivity for one transmitter and all receiver locations m with respect to a fixed model volume n providing one *column* of the sensitivity matrix in eq. (2) (i.e., m runs through all values whereas n remains fixed).

2.3 Calculation of the Sensitivity by Perturbation

The differential form $\partial V_m/\partial\rho_n$ may be substituted by a difference expression $\Delta V_m/\Delta\rho_n$ with $\Delta\rho_n = \rho_n' - \rho_n''$ and ρ_n'' as a perturbed resistivity, if $\Delta\rho_n \ll \rho_n'$. Thus, by changing the resistivity of a block by a "small" amount and subtracting the perturbed potential responses from the unperturbed ones, an approximation of the sensitivity is obtained. Both potential distributions are calculated using FD forward modeling. As in section 2.2, one column of the Jacobian matrix is obtained.

2.4 Analytical Calculation of the Sensitivity for a Homogeneous Halfspace

For a homogeneous halfspace, the current density obeys the analytical law (here again for x-direction)

$$j_x = -\frac{I}{4\pi}\frac{\partial}{\partial x}\left(\frac{1}{|r|} + \frac{1}{|r'|}\right) \quad , \tag{11}$$

which is derived from Ohm's law, $\boldsymbol{E} = -\nabla V$ and the analytical expression for the potential at an arbitrary position within the conducting halfspace (at the surface or subsurface). The $\frac{1}{|r'|}$ term is due to an image source at distance $|r'|$ from the receiver within the non-conducting "air space", $|r|$ is the distance between source and receiver.

The sensitivity can now be determined using the sensitivity theorem of Geselowitz (eq. 7) and the current density from eq. (11). The integration over the perturbed volume has to be carried out numerically, which in this case has been done by Gaussian quadrature using Gauss-Legendre polynomials (Press et al., 1986). There are no preferences concerning the calculation of rows or columns of the Jacobian. The amount of numerical work is equal. Rows or columns are simply selected by the choice of the running index.

2.5 The Methods in Comparison

With each execution, the first FD method (section 2.1) provides a row of the sensitivity matrix, whereas the second one (section 2.2) yields a column. Both methods use two forward runs for the calculation of the first set of sensitivities; the second method, however, only needs one further forward run for each additional set, thus, being advantageous to the first one as far as the cumulative amount of numerical work is concerned. Depending on individual conditions and requirements both methods are subject to trade-off, though. Method three (section 2.3) is mainly for crosscheck reasons because of its simplicity. The advantages of the analytical approach (section 2.4) lie in its speed and accuracy. The speed is of particular interest if it comes to numerical inversion, where the whole sensitivity matrix has to be determined. Although one forward modeling using the FD-method of section 2.2 is carried out, e.g., in

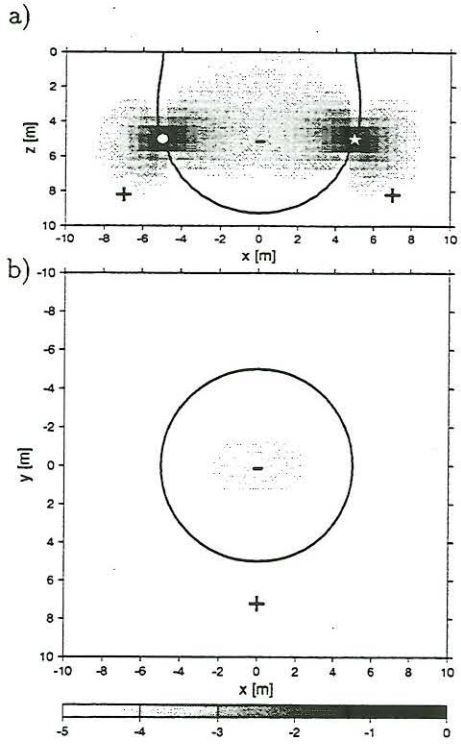

Figure 1: *Logarithmic normalized sensitivity for a subsurface pole-pole configuration in a homogeneous halfspace. The plot shows one row of the sensitivity matrix. Note the zone of negative sensitivity forming a tube-like shape.*

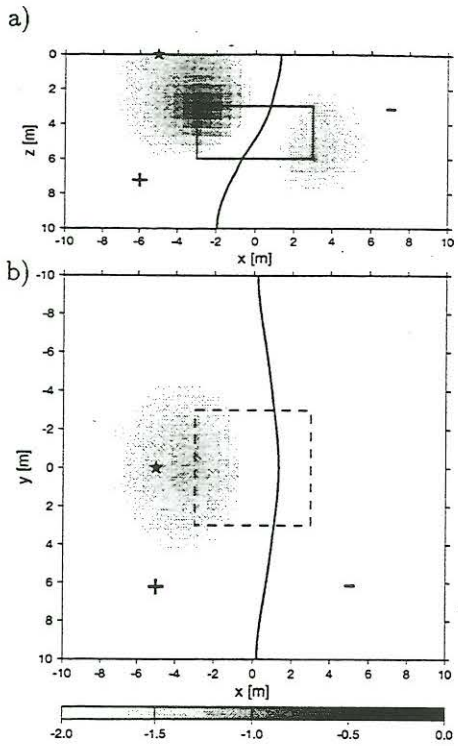

Figure 2: *Logarithmic normalized sensitivity with respect to a buried cube. The plot shows one column of the sensitivity matrix.*

about 9 s on a Sun Sparc Ultra for a grid of 41 × 41 × 21 nodes, the time needed to calculate every individual sensitivity for each cell with respect to each node and one source location totals approximately 80 hours. This is way too slow under all circumstances and, therefore, not feasible. To achieve a starting value for the iterative process in non-linear inversion, the analytical method only needs 14 min to achieve the same set of sensitivities, but only for a homogeneous structure, though. The method might be even speeded up, if the applied numerical integration method, here Gaussian quadrature, is carried out using less function values (see Loke and Barker, 1996).

3 Sensitivity Distributions

In the following, the sensitivity distribution is shown only for a subsurface pole-pole arrangement. The 3D space is depicted using orthogonal sections along the surface and the vertical through the sources. For better illustration, the sensitivity is displayed as a logarithmic property normalized by division of its greatest value. Since the reciprocity principle is valid, receiver and transmitter is interchangeable.

Fig. 1 shows the sensitivity for a pole-pole configuration at a subsurface location. Since the electrode configuration is fixed, the graph shows the sensitivity as a function of the location of a cell, i.e., one row of the sensitivity matrix (eq. 2) is plotted. Fig. 1a displays the vertical section through the source locations. The solid line marks the zero sensitivity line which is associated with a change of sign. A zone of negative sensitivities stretches out between the electrodes forming a tube-like shape that opens toward

the surface. Generally, the absolute value of the sensitivity increases as one approaches the electrode locations. Fig. 1b shows the sensitivity along the surface where the zero sensitivity line forms a circle through the points located perpendicularly above both electrode locations. In 3D space, the negatively sensitive region thus forms a cylindrical shape with a semi-spherical or bowl-like structure at the bottom. The change in resistivity of any volume element within this zone is associated with a sign-reversed change in apparent resistivity. The cylindrical structure is maintained as long as the electrodes are buried at finite depth. With increasing depth, the surface sensitivity values decrease as a matter of course. With $d \to \infty$ they converge towards zero and the change of sign at the surface disappears. The response then assumes the full space solution containing a closed sphere of negative sensitivities. The region of negative sensitivities also assumes a closed sphere even in presence of the surface at finite distance, if the pole-pole configuration is oriented vertically, i.e., if the surface normal and the normal on the connecting line between the poles are orthogonal.

Another interesting way of looking at the sensitivity distribution is obtained by exchanging the running indices. All previous figures show the sensitivity with respect to a fixed source/receiver configuration. Thus, the index of the cell location n runs through all possible values being associated with one row of the sensitivity matrix. Keeping the location of the cell or resistivity block fixed and letting the receiver index m cycle through all values of the 3D grid, we generate the sensitivity map shown in Fig. 2a and b, which displays one column of the sensitivity matrix along a vertical section and the surface. The fixed resistivity block is a rectangular 3D prism centered at a depth of 4.5 m at $x = y = 0$ m with sides 6 m long in the x- and y-directions, and 3 m in the z-direction. The result is obtained performing explicit sensitivity forward modeling as described in section 2.2. The sensitivity is now a function of the receiver position. The bended solid line again indicates zero sensitivity. The source is located at the surface. For receiver positions on the right-hand side of the zero sensitivity line, the sensitivity becomes negative which is in accordance with Fig. 1, where the negative area is between the electrodes. Note that a configuration using a receiver electrode along the zero sensitivity line would not respond to resistivity changes of the block, even if the receiver is located within the block itself.

This result agrees well with the theory of charge accumulation at conductivity contrasts. In case of a positive current I flowing from a resistive into a conductive medium, we obtain an accumulation of negative charges along the boundary due to the continuity of the normal components of the current density and the continuity of the tangential components of the electric field (Li and Oldenburg, 1991). Within a region of additionally accumulated negative charges the measured positive potential is diminished yielding decreased apparent resistivities. We now find a positive maximum of the sensitivity, i.e., a decreased apparent resistivity at the upper left-hand edge of the conducting block in Fig. 2a which is in agreement with the results presented by Li and Oldenburg (1991, Fig. 6a-f).

Of course, the depiction of sensitivities in the way of Fig. 2a is equivalent to the one of equiperturbation lines presented, e.g., by Shima (1992) for the 2D case. However, the 2D response deviates significantly from the 3D one as we will see later in section 4.2.

4 The Influence of Resistivity Contrasts on the Sensitivity

So far, all shown sensitivities are for the homogeneous halfspace. Of course, a non-uniform conductivity structure will deform the sensitivity distribution. However, it is shown that the homogeneous case gives a good approximation or first guess for a range of moderate conductivity changes. In the first place, the forward modeler's interest is focussed on the spatial extensions of negatively or positively sensitive

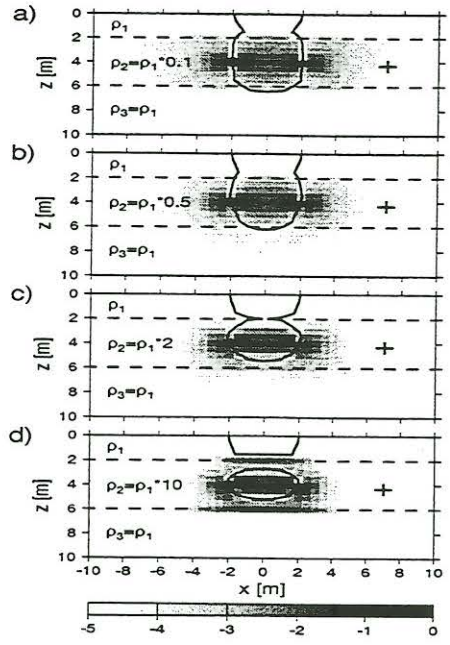

Figure 3: *Logarithmic normalized sensitivity for a subsurface pole-pole configuration buried in the middle layer of a three-layer model.*

regions to apply the appropriate resistivity changes to the model during the interpretation process and achieve a better match to the data. From certain conductivity contrasts on, though, the spatial pattern of the homogeneous case is broken up so that the sensitivity distribution has to be calculated individually to gain information on its structure. General predictions are difficult to quantify. Nevertheless, the following examples give an overview of what to expect for some classes of more realistic inhomogeneous structures.

4.1 A Three-Layer Earth

In order to investigate in greater detail the influence of resistivity contrasts on the sensitivity, some common inhomogeneous structures are studied. In particular, we consider a downhole electrode arrangement typically applied in mining environments using a subsurface pole source and receiver usually located within two boreholes. First, a three-layer earth (ρ_1, ρ_2, $\rho_3 = \rho_1$) including the pole-pole arrangement in its middle layer is examined. The resistivity ρ_2 of the middle layer is gradually changed from $\rho_2/\rho_1 = 0.1$ (conductive layer) to $\rho_2/\rho_1 = 10$ (resistive layer) using four steps. The results are shown in Fig. 3 depicting the sensitivity for a fixed transmitter/source combination as a function of space (corresponding to Fig. 1a). The FD method described in section 2.1 is well suitable for this kind of problem and has therefore been used to calculate the results. For the conductive layer, the spatial pattern resembles the homogeneous one even for a conductivity contrast of $\rho_2/\rho_1 = 0.1$ (Fig. 3a,b). In contrary, the changes are more drastic if the middle layer becomes increasingly resistive. With moderate contrasts ($\rho_2/\rho_1 = 2$, Fig. 3c), we already observe a significant narrowing of the negative zone at the boundary between the first and second layer. With further increasing resistivity, the negative zone is even split up in two (Fig. 3d). This is physically comprehensible, if we consider the current density again. In the case of the conductive layer, the current is channeled within the layer. The component of the current density normal to the layer boundaries is increased when the neighboring layers are becoming more conductive. Therefore, a greater charge is accumulated at the boundaries disturbing the potential distribution along the boundaries.

In summary, the homogeneous earth approach is a sufficient approximation for inhomogeneous cases, in which the source is located within the conductor and the conductivity contrast is less than 1:10. More significant alterations of the spatial sensitivity pattern are encountered for even lower contrasts, when the source is located within resistive material.

4.2 A Rectangular Prismatic Body

In this section a typical crosshole situation is investigated (Fig. 4). A rectangular 3D prismatic body, whose sides are 6 m long, is centered between two boreholes at (x,y,z)=(0 m, 0 m, 5 m). The left-hand borehole contains the transmitter at a depth of 5 m (circle) and the potential log is run along the so

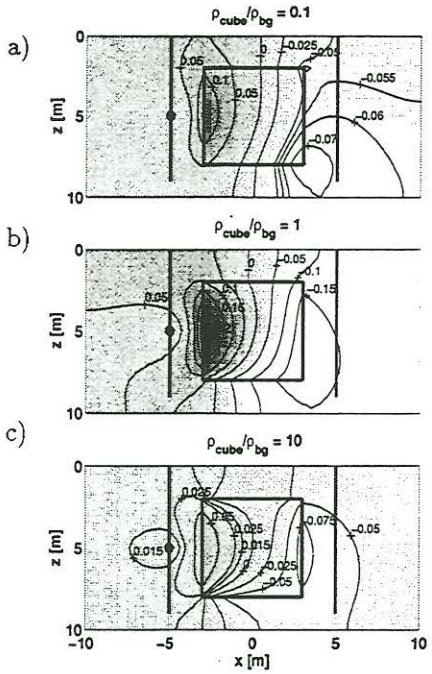

Figure 4: *Contour plots for the sensitivity with respect to a 3D rectangular prismatic body as a function of the receiver pole.*

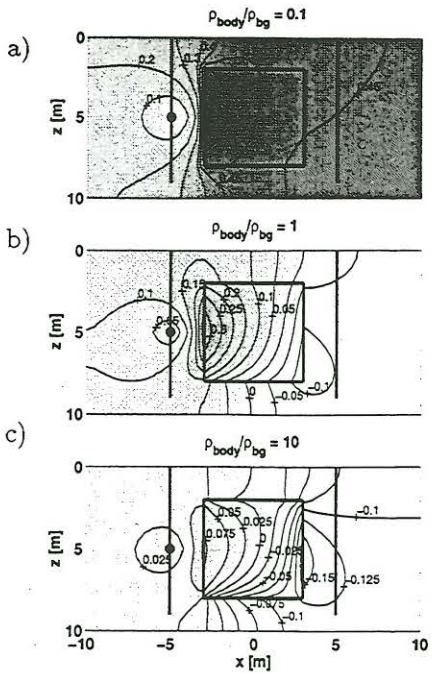

Figure 5: *Contour plots for the sensitivity as a function of the receiver pole with respect to a 2D rectangular body striking in y-direction.*

called receiver borehole on the right-hand side. For simplicity, the boreholes positioned at (x,y)=(±5 m, 0 m) are straight and vertical and are indicated by the lines left and right from the body.

In a first sequence, three different resistivities are assigned to the body and their responses are investigated in terms of sensitivity (Fig. 4a-c). For this purpose, the method outlined in section 2.2 is appropriate, because we obtain the sensitivity with respect to the body as a function of the receiver position throughout the conductive halfspace. The results are presented as vertical sections in the way of Fig. 2, but normalized by the factor ρ_{cube}/V_i, where V_i is the potential at node i and ρ_{cube} is the resistivity of the body. Thus, e.g., $\Phi = 1$ stands for direct proportion and $\Phi = -1$ indicates inverse proportion. In each plot, a positive maximum of the sensitivity occurs at the side facing the source, whereas a negative minimum appears at the far side of the cube. The sensitivity pattern varies with the body's resistivity in amplitude as well as in its spatial behavior. The sensitivity maxima are greatest when the body's resistivity is equal to the background resistivity ($\rho_{cube}/\rho_{bg} = 1$, Fig. 4a) or, in other words, the sensitivity with respect to the body decreases with increasing difference to the background resistivity. Additionally, the negative minimum is dislocated to greater depths as ρ_{cube}/ρ_{bg} decreases. The asymmetry is related to the presence of the surface not allowing any current to flow into the air space. The decrease of its influence with the body's increasing resistivity might be confusing at first glance, because the current system is obviously channeled between the resistive body and the surface. But according to the sensitivity theorem (eq. 7), the inner product of the current densities are integrated over the body's volume. Therefore, a conductive body that channels the current inside its volume rather introduces the asymmetry into the sensitivity structure than a resistive body.

This is not the case for 2D structures. If we carry out the same investigation using a 2D body, we obtain significantly different results. Fig. 5 depicts vertical sections analogous to those of Fig. 4, but now for a 2D body with strike in y-direction. While the resistive body (Fig. 5c) and the body of background resistivity (Fig. 5b) resemble their corresponding 3D cases, only showing greater extreme values, the response of the conductive body (Fig. 5a) is strongly deviating (compare to Shima, 1992). The negative

minimum is completely missing and the positive maximum is extremely strong showing values of $\Phi > 0.6$ at the side of the cube facing the source (see Spitzer & Chouteau, 1996).

This shows that 2D approximations for cases implying 3D conductive bodies are not valid and should be considered with great caution. The 2D and 3D responses are better compatible if the source is located within conductive material, i.e., when the body is resistive.

5 Conclusions

The sensitivities play key roles in understanding the physics of the DC potential and its response to subsurface resistivity changes. This is of fundamental concern for the interpretation of any kind of geoelectrical depth investigation. Especially, subsurface sources yield sensitivity patterns which should be carefully studied and taken into account when interpreting field data sets. The aim of this paper is to describe a number of methods for calculating the sensitivity in three-dimensional homogeneous and arbitrarily inhomogeneous cases and to give an example of how these patterns are shaped for a common pole-pole configuration in homogeneous cases. For inhomogeneous media, the representative example of a three-layer case suggests that the homogeneous response is approximately valid for a range of moderate conductivity contrasts less than 1:10, when the source is located within the conductor. However, a significant deformation of the shown sensitivity distributions is inevitable in presence of high conductivity contrasts and should therefore be considered during the interpretation process, especially, when the source is located within resistive material in the vicinity of conductors. Further model studies for crosshole environments have shown that 2D approximations do not hold for conductive 3D bodies, whereas 2D and 3D approximations show better agreement for resistive bodies.

Acknowledgments.

I would like to thank Liming Yu and Michel Chouteau, École Polytechnique, Montreal, for the very pleasant and fruitful cooperation. Discussions with Doug Oldenburg, University of British Columbia, Vancouver, Ashok Agarwal, University of Victoria, and David Boerner, Geological Survey of Canada, Ottawa, were highly appreciated. Furthermore, I am grateful to both reviewers, Andreas Weller, TU Clausthal, Germany, and Randy Mackie, GSY-USA Inc., San Francisco, for their constructive and clarifying comments. The work was funded by NSERC, TVX Gold, and Golden Knight (TVX Gold/Golden Knight Chair in Borehole Geophysics contribution # 9702) and the Deutsche Forschungsgemeinschaft (Research Grant Spi 356/2-1).

References

Barker, R.D., 1979. Signal contribution sections and their use in resistivity studies, *Geophys. J. R. astr. Soc.*, **59**, 123 – 129.

Boerner, D.E., and West, G.F., 1989. Fréchet derivatives and single scattering theory, *Geophys. J. Int.*, **98**, 385 – 390.

Brewitt–Taylor, C.R., and Weaver, J.T., 1976. On the finite difference solution of two–dimensional induction problems, *Geophys. J. R. astr. Soc.*, **47**, 375 – 396.

Geselowitz, D.B., 1971. An Application of Electrocardiographic Lead Theory to Impedance Plethysmography, *IEEE Trans. Biomed. Eng.*, **BME-18**, 39 – 41.

Hestenes, M.R. and Stiefel, E. 1952. Method of conjugate gradients for solving linear systems, *J. Res. Nat. Bur. Standards* **49**, 409 – 436.

Lanczos, C., 1961. Linear Differential Operators, Van Nostrand, London.

Li, Y., and Oldenburg, D.W., 1991. Aspects of charge accumulation in d.c. resistivity experiments, *Geophys. Prosp.*, **39**, 803 – 826.

Loke, M.H. and Barker, R.D., 1996. Practical techniques for 3D resistivity surveys and data inversion, *Geophys. Prosp.*, **44**, 499 – 523.

McGillivray, P.R., and Oldenburg, D.W., 1990. Methods for calculating Fréchet derivatives and sensitivities for the non-linear inverse problem: a comparative study, *Geophys. Prosp.*, **38**, 499 – 524.

Noel, M., and Xu, B., 1991. Archaeological investigation by electrical resistivity tomography: a preliminary study, *Geophys. J. Int.*, **107**, 95 – 102.

Oldenburg, D.W., 1978. The interpretation of direct current resistivity measurements, *Geophysics*, **43**, 610 – 625.

Park, S.K. and Van, G.P., 1991. Inversion of pole–pole data for 3-D resistivity structure beneath arrays of electrodes, *Geophysics*, **56**, 951 – 960.

Press, W.H., Teukolsky, S.A., Vetterling, W.T., and Flannery, B.P., 1986. Numerical recipes, Cambridge University Press.

Sasaki, Y., 1994. 3-D resistivity inversion using the finite element method, *Geophysics*, **59**, 1839 – 1848.

Shima, H., 1992. 2-D and 3-D resistivity image reconstruction using crosshole data, *Geophysics*, **57**, 1270 – 1281.

Smith, N.C. and Vozoff, K. 1984. Two–dimensional DC resistivity inversion for dipole–dipole data, *IEEE Transactions on Geoscience and Remote Sensing* **GE-22**, 21 – 28.

Spitzer, K., 1995. A 3D finite difference algorithm for DC resistivity modeling using conjugate gradient methods, *Geophys. J. Int.*, **123**, 903 – 914.

Spitzer, K., and Chouteau, M., 1996. Investigations on the apparent resistivity, sensitivity, and IP frequency effect for crosswell arrangements in three-dimensional environments, Extended Abstract Book of the Pre-Convention Workshop "The Role of In-Mine Geophysics in Resource Evaluation" held on Nov. 10, 1996, at the 66th Annual Meeting of the Society of Exploration Geophysicists in Denver, Colorado.

Spitzer, K., and Kümpel, H.-J., 1997. 3D FD resistivity modeling and sensitivity analyses applied to a highly resistive phonolitic body, *Geophys. Prosp.*, **45**, 963 – 982.

Weller, A., Gruhne, M., Seichter, M., and Börner, F.D., 1996. Monitoring Hydraulic Experiments by Complex Conductivity Tomography, *European Journal of Environmental and Engineering Geophysics*, **1**, 209 – 228.